

Field-induced non-Fermi-liquid resistivity of stoichiometric YbAgGe single crystals

P. G. Niklowitz,* G. Knebel, and J. Flouquet

*Département de Recherche Fondamentale sur la Matière Condensée,
SPSMS, CEA Grenoble, 38054 Grenoble Cedex 9, France*

S. L. Bud'ko and P. C. Canfield

*Ames Laboratory, Iowa State University, Ames, Iowa 50011, USA and
Department of Physics and Astronomy, Iowa State University, Ames, Iowa 50011, USA*

(Dated: June 23, 2018)

We have investigated hexagonal YbAgGe down to 70 mK by measuring the magnetic-field and temperature dependence of the resistivity ρ of single crystals in fields up to 14 T. Our results extend the $H - T$ phase diagram to the lowest temperatures for H applied in the basal plane and along the c -axis. In particular, critical fields for the suppression of several magnetic phases are determined. The temperature dependence of $\rho(T)$ is unusual: whereas at low H , $\rho(T)$ reveals a temperature exponent $n \geq 2$, we find $1 \leq n < 1.5$ and strong enhancement of the temperature dependence of $\rho(T)$ close to and beyond the highest critical field for each field direction. For H applied in the basal plane, at high fields a conventional T^2 dependence of $\rho(T)$ is reached above 10 T accompanied by an approach to saturation of a strong drop in the residual resistivity. YbAgGe appears to be one of few Yb-based stoichiometric systems, where quantum-critical behaviour may be induced by a magnetic field.

PACS numbers: 71.27.+a; 75.30.Mb; 75.47.-m

Keywords: field-induced quantum phase transition, magnetoresistance, electrical resistivity, heavy-fermion systems, Kondo lattice, spin fluctuations, YbAgGe

I. INTRODUCTION

Metals at the border of magnetic order often show deviations from the thermodynamic and transport properties predicted by Fermi-liquid (FL) theory, the standard model of metals. Materials can be tuned through the magnetic quantum phase transition by application of pressure or doping. A different route lies in tuning materials by the application of a magnetic field. Field-induced quantum phase transitions have been studied in several groups of systems: (i) the extensively studied materials with a metamagnetic transition CeRu₂Si₂,^{1,2} Sr₃Ru₂O₇,³ UPt₃,⁴ or URu₂Si₂,⁵ (ii) Ce₂IrIn₈, where non-Fermi-liquid behaviour might be linked to field-induced magnetic order other than ferromagnetic order;⁶ (iii) CeCoIn₅, where non-Fermi-liquid behaviour has been found at the upper critical field of the superconducting phase, below which superconductivity and antiferromagnetism seem to coexist;⁷ (iv) antiferromagnetic metals where spontaneous magnetic order gets suppressed. Here we focus on group (iv). Field-induced quantum critical points (QCPs) have already been identified in several Ce-based antiferromagnetic heavy-fermion systems, including CeCu_{6-x}Ag_x or CeCu_{5.8}Au_{0.2}.^{8,9,10} Among Yb-based stoichiometric heavy-fermion systems, only YbRh₂Si₂ has been reported to show field-induced quantum-critical behaviour.^{11,12,13}

YbAgGe offers a new possibility for a study of the rich f -electron physics at a field induced magnetic quantum phase transition in a stoichiometric compound. YbAgGe has recently been recognised as a new heavy-fermion sys-

tem with a linear specific heat coefficient γ of a few hundred mJ/molK² at low temperatures and a Kondo temperature $T_K \approx 25$ K.^{14,15} Two antiferromagnetic transitions, which are found at low temperatures already at ambient conditions, can be fully suppressed within the experimentally well accessible magnetic field regime of less than 10 T.¹⁶

YbAgGe orders in the hexagonal ZrNiAl-type structure.¹⁴ The Yb³⁺ ions are exposed to a crystal field with an orthorhombic point symmetry, which splits their eight-fold $J = 7/2$ multiplet into four doublets. Inelastic neutron scattering revealed a crystal-field excitation at 12 meV, which is also visible as a Schottky anomaly in the specific heat at 60 K.^{15,17} The specific heat data can be explained, if it is assumed that the Schottky anomaly corresponds to the lowest crystal-field excitation. However, such a model does not explain the susceptibility and some uncertainty on the crystal-field scheme remains. Magnetisation measurements show clear anisotropy growing to $\chi_{ab}/\chi_c \approx 3$ at low temperatures.^{14,15} Saturation of the magnetisation close to 15 T is only found when the field is applied in the easy plane. Above T_K the susceptibility derived from the magnetisation data follows the Curie-Weiss law with an effective moment of $4.4\mu_B$ (close to the free-ion value for Yb³⁺ of $4.5\mu_B$) and with a Weiss temperature $\Theta = -30$ K, which suggests antiferromagnetic interactions between the moments. Below T_K the susceptibility levels off and shows a weak maximum at about 4 K^{14,15}.

At low temperatures, two transitions to antiferromagnetic phases (AF1 at the lowest temperatures and AF2) are observed at zero field.^{14,16,18,19,20} A first transition

is located at $T_1 = 0.65$ K, which has been observed as a sharp peak in the heat capacity and as a jump in the resistivity. A clear hysteresis in the heat capacity and in the resistivity shows that the transition is first order.^{14,16,18} At $T_2 = 0.9 \pm 0.1$ K there is a second transition, which shows up as a relatively broad feature in the specific heat and as a broad change of slope in the electrical resistivity. Further information on the nature of the antiferromagnetic phases comes from heat capacity measurements and neutron scattering studies. The entropy calculated from the heat capacity reaches only 5% of $R \ln 2$ at 1 K and $R \ln 2$ close to 25 K, which suggests that any ordered moment is only of the order of $0.1 \mu_B$.¹⁴ Recently, neutron diffraction at zero field revealed for the AF1 phase the commensurate ordering wave vector $(1/3, 0, 1/3)$ and indicated moment orientation predominantly in the basal plane.¹⁹ The AF2 phase above T_1 shows incommensurate order and its suppression at T_2 happens via a second-order transition.²⁰ Inelastic neutron scattering (Ref. 19) was found to be quasielastic and revealed fluctuations predominantly in the basal plane with a temperature dependence characteristic of a heavy-fermion material. At low temperatures, however, an anomalous \mathbf{q} -dependence of the linewidth $\Gamma(\mathbf{q})$ was found, which varies along the c -axis but which is constant in the basal plane. The origin of this anomalous \mathbf{q} -dependence might come from the structural particularity of YbAgGe that the magnetic Yb-ions lie on a distorted Kagome lattice with the potential for magnetic frustration.

YbAgGe completes a trend, which can be observed in RAgGe compounds, where R stands for various rare earths.¹⁴ In going from R=Tb to R=Yb the magnetic anisotropy changes from being axial $\chi_{ab}/\chi_c < 1$ to being planar $\chi_{ab}/\chi_c > 1$. Furthermore, the magnetic transition temperatures decrease with an approximate de-Gennes scaling. However, in YbAgGe, the large value for the linear heat-capacity coefficient γ indicates that magnetic exchange connected with the hybridisation between f -electrons and conduction electrons influences the value for the magnetic transition temperatures and it is by accident that YbAgGe does not significantly deviate from de-Gennes scaling of the RAgGe series. The large γ value also suggests that YbAgGe should be close to quantum phase transitions and possibly a quantum critical point.

The proximity of quantum phase transitions has already been pointed out by the exploration of the H^a - T and H^c - T phase diagram (a and c indicate the crystal axis, along which the magnetic field was applied).^{16,18,20} In addition to the above mentioned signals in the heat capacity and resistivity indications of the two transitions are also visible in the magnetoresistance and in the magnetization. For both field directions applied magnetic fields of less than 10 T are sufficient to reach the critical fields H_c necessary to suppress antiferromagnetic magnetic order. From neutron scattering experiments H_{c2}^a (H_{c2} for $H \parallel a$) was found to be 3 T.²⁰ However, features in the resistivity, heat capacity, and magnetization¹⁸ extrapolate to a further critical field H_{c3}^a . Furthermore, the

critical field H_{c3}^a is the starting point of the lines in the $H - T$ phase diagrams, which is defined by features in the Hall resistivity, and which shifts to higher field with increasing temperature.²¹

This paper describes detailed measurements of low-temperature properties of YbAgGe in a magnetic field. The measurements cover the field range up to 14 T with the field applied in the easy plane and along the c -axis. The current has been applied along two crystallographic directions as well. The corresponding $H^a - T$ and $H^c - T$ phase diagrams are extended to 70 mK, which allows a precise determination of the critical fields. One specific aim was to search for field-induced quantum critical phenomena. Specific heat and resistivity measurements down to 0.4 K indicated the existence of quantum critical fluctuations: in approaching H_{c3}^a , γ and the strength of the low-temperature dependence of the resistivity are enhanced and the resistivity deviates more strongly from the quadratic Fermi-liquid form.¹⁶ This low-temperature study shows quite dramatic changes in the temperature dependence of the resistivity just above these critical fields, which are typically observed close to a quantum critical point. However, an unconventional form of the resistivity has been detected over unusually large H -intervals down to very low temperatures. Additionally, a strong field dependence of the residual resistivity with a large enhancement at low fields has been observed.

II. EXPERIMENTAL

The YbAgGe samples measured in this study were grown from high-temperature ternary solutions rich in Ag and Ge. The samples had the form of clean hexagonal cross-section rods of several millimeters length and 0.3-0.8 mm² cross section. Their structure and the absence of impurity phases were confirmed by powder X-ray diffraction (details of the sample growth are found in Ref. 14). The ac-resistance was measured by a standard four-terminal method ($f \approx 28$ Hz, $I = 25 - 100 \mu\text{A}$). Gold wires were attached to the samples by spot-welding using the smallest possible voltages for welding. The samples were cleaned in HNO₃ before attaching the gold wires to remove residual flux and in general to avoid damage to the sample during spot-welding. For measurements with the current in the plane thin slices with a thickness of 80-300 μm were cut off the sample rods. For the in-plane measurements the current was approximately sent along the [100] direction. $\rho(T, H)$ was measured down to 70 mK in a dilution refrigerator containing an Oxford Instruments 18 T superconducting magnet. The sample was orientated such that the field was either applied along [001] or in the plane approximately along [100]. A low-temperature RuO₂ thermometer was initially only calibrated in zero field. The in-field calibration was done by regulating a capacitor to a constant value during field sweeps. The optimal balance in the calibration proce-

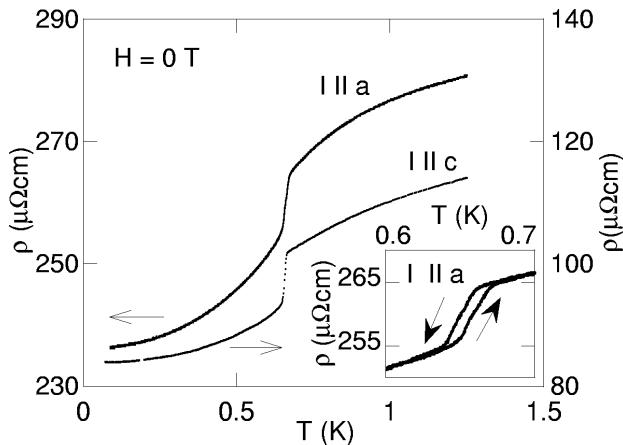


FIG. 1: Temperature dependence of the resistivity with no applied field. No qualitative change in the mK range is found upon altering the current direction. However, the resistivity is anisotropic with larger in-plane values. In the inset the first order character of the transition between the AF1 and AF2 phase is shown. Arrows indicate the direction of the temperature sweeps.

ture between eddy-current heating and a drift of the capacitance resulted in a temperature error of 3 mK for the RuO_2 thermometer. This is the dominant error in the resistivity measurements and determines the errors of temperature exponents in the analysis of the resistivity data. The resistivity was determined in temperature sweeps with a sweep rate of 0.2 K/h and in field sweeps with a sweep rate of 3 T/h. Due to the hysteretic character of the transition $T_1(H)$ we specify here that in the hysteretic region results have been gained from up-sweeps in field and temperature unless otherwise indicated. Furthermore, before each up-sweep in temperature the sample was zero-field cooled.

III. RESULTS

In Figure 1, we show the resistivity of YbAgGe at zero field. For the in-plane as well as for the c -axis resistivity we find a large jump of the order of $10 \mu\Omega\text{cm}$ at $T_1(H=0\text{T}) = 666 \pm 5 \text{ mK}$ as signature of the transition between the AF1 and AF2 phase. The hysteresis in the inset of Figure 1 confirms the first-order character of this transition. No sharp signal for T_2 of the second transition at around 1 K can be resolved. A broad change of slope of $\rho(T)$ around T_2 is more evident in previous studies, which reached to higher temperatures.^{14,16,18} The in-plane resistivity is in general higher and shows a stronger temperature dependence. The difference might partially arise from the error in the estimation of the small sample geometry. For the resistance ratio (RRR) we find 2.7 and 3.4 for the current directions $I||a$ and $I||c$, respectively. The residual resistivity ρ_0 is 2.8 times higher in the plane than along the c -axis. The order of magnitude

of ρ_0 in our measurements is comparable to values found in previous zero-field studies. Values for $T_1(H=0)$ from previous studies, ranging from 0.55 K to 0.65 K, are close to our result as well.^{14,15,16,17,18} However, we cannot confirm the previously found sudden rise of the in-plane resistivity towards lower temperatures at T_1 .¹⁸ Differences in the sample growth technique might explain the discrepancies.

In the following we present the resistivity of YbAgGe in a magnetic field. We measured the resistivity for the combinations of field and current direction $H||a$ with $I||a$ or $I||c$, and $H||c$ with $I||c$. Since it will be seen that for $H||a$ the temperature dependence $\Delta\rho = \rho - \rho_0$ is rather independent of the current direction we discuss the results for the two current directions in parallel. For the same reason we have done only measurements with one current direction in the case of $H||c$. The resistivity curves $\rho(T)$ have been analysed by fitting $\rho(T) = \rho_0 + cT^n$ (ρ_0 , c , and n are fitting parameters) over the largest temperature interval, which allows a single-power-law fit. This analysis is used to determine the temperature-independent residual resistivity ρ_0 , and separate it from the temperature dependent part $\Delta\rho = cT^n$, where c is a constant and n the temperature exponent of the resistivity.

A. $H||a$

In this section we present results of the temperature and field dependence of the resistivity for the case $H||a$. Figure 2a contains $\rho(T)$ curves at small fields showing signatures of the first-order transition between the AF1 and AF2 phase and their suppression to low temperatures towards higher fields. Up to its suppression below 70 mK at 2.5 T the first-order transition is marked by the onset of a large drop of $\rho(T)$ at $T_1(H||a)$, similar to its transition signal at zero field. Figure 2b shows a much less visible feature in $\rho(T)$ that manifests itself only as a weak shoulder at $T_3(H||a)$. This shoulder in $\rho(T)$ can be identified up to 4.6 T. Signatures corresponding to $T_1(H||a)$ and $T_3(H||a)$ are clearly seen in the magnetoresistance (Figure 3). The first-order transition appears as the onset of a drop towards low field of $\rho(H||a)$ at $H_1^a(T)$, similar to its feature in $\rho(T)$. The feature at $T_3(H||a)$ shows up as a shoulder at $H_3^a(T)$ and is better visible at lower temperatures. A broad bump indicates a further transition at $H_2^a(T)$, which can be followed up to $\approx 500 \text{ mK}$. At low T there might be a fourth feature close to $H_1^a(T)$, which has to be confirmed by even more detailed magnetoresistance measurements at low temperatures. The signatures of transitions in $\rho(T, H^a)$ shown in Figures 2 and 3 and further results of $\rho(T, H^a)$ measurements, which are not explicitly shown, allow us to draw the H^a - T phase diagram of YbAgGe (Figure 12a). The phase diagram shows the clear correspondence between signatures in temperature and field sweeps of the resistivity. The AF1 phase is fully suppressed at H_{c1}^a below 3 T. An uncertainty seems to remain from the observation that the suppression be-

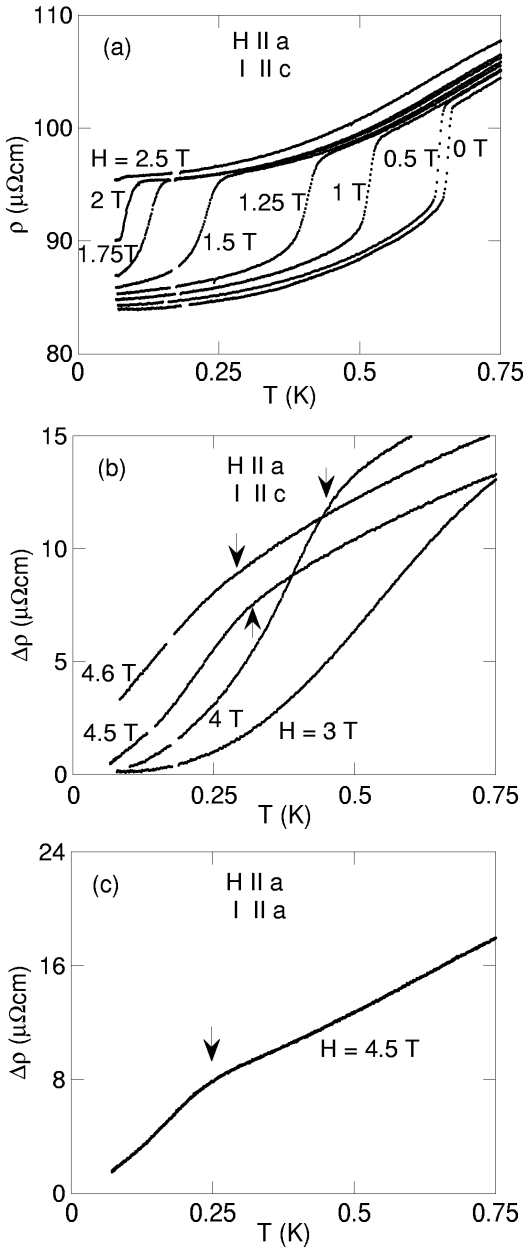


FIG. 2: Signatures in the temperature dependence of the resistivity $\rho(T)$ for $H\parallel a$. (a) T_1 (onset of drop in ρ) is gradually suppressed with field and fully disappears at 2.5 T. (b),(c) Signatures of T_3 : the shoulder (marked by arrows) also is suppressed with increasing field. In parallel, the initial slope of $\Delta\rho(T)$ increases from 3 to 4.6 T.

comes less rapid below 200 mK. However, this slowdown of the suppression of T_1 with increasing field is not observed in neutron scattering and $H_{c1}^a = 1.8 \pm 0.1$ T.²⁰ The discrepancy might have been caused by the long relaxation to equilibrium of YbAgGe around the first-order transition, which was observed in the neutron-scattering experiment. The AF1 phase is followed by the AF2 phase with its critical field $H_{c2}^a = 3.0 \pm 0.1$ T, and by a region III with unknown magnetic properties, which exists up

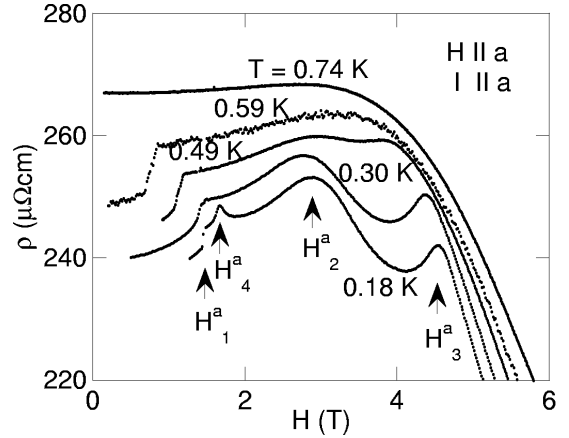


FIG. 3: Signatures in the field dependence of ρ for $\rho(H\parallel a)$ at various temperatures. The field sweeps at different temperatures reveal the first-order transition (H_1^a , onset of jump in ρ), the second-order transition (H_2^a , bump) and a further feature (H_3^a , onset of strong drop of ρ towards high fields), which indicates a further transition. A fourth feature (H_4^a), has yet to be confirmed by further measurements.

to $H_{c3}^a = 4.9 \pm 0.1$ T. Figure 12a shows how the results of this study extend the phase diagram, obtained by previous thermodynamic and transport measurements down to 0.4 K. There is good agreement between our and previous data in the overlap region from 0.4 to 0.75 K.^{16,18,21} The shape of signatures of the two transitions at T_1 and T_3 in our and previous resistivity measurements is very similar as well.

We now give a more quantitative description of $\rho(T)$ of YbAgGe when $H\parallel a$. In the inset of Figure 4a the field dependence of $\rho(75$ mK) and ρ_0 can be seen. On the shown large resistivity scale both curves are similar. $\rho_0(H\parallel a)$ drops strongly from low-field values of about $90 \mu\Omega\text{cm}$ to $25 \mu\Omega\text{cm}$ at 14 T. ρ_0 starts to saturate at fields $H\parallel a$ of the order of 10 T, at which the susceptibility is strongly reduced.¹⁶

Figure 2 and 4 for $I\parallel c$ and Figure 5 for $I\parallel a$ demonstrate the development with $H\parallel a$ of the magnitude of the low-temperature dependence of $\Delta\rho$. The field dependence of the temperature exponent n obtained from power law fits is shown in Figure 6. At fields clearly below H_{c3}^a ($H\parallel a < 4.5$ T) we find values for n close to or above the Fermi-liquid value 2. An approximately quadratic resistivity is also observed at high fields $H\parallel a > 10$ T. Around the highest critical field $H_{c3}^a = 4.9$ T we find $n = 0.9 \pm 0.2$. It has to be noted that $n \approx 1$ not only right at H_{c3}^a but in an extended field region up to 7 T, which agrees with the observation of a linear $\Delta\rho$ in a wider field range above 0.4 K.¹⁶

Figure 6 also shows the development with $H\parallel a$ of the magnitude of the temperature dependence of the resistivity $\Delta\rho$ at low T . $\Delta\rho(T')$ at a low temperature T' is a measure of the amount of low-energy excitations present in a material, since they can act as scatterers of the con-

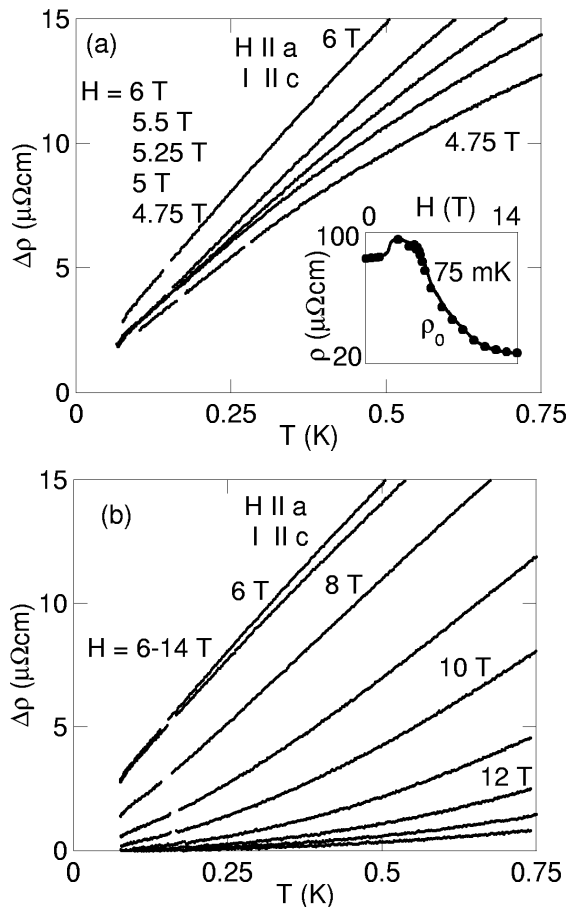


FIG. 4: Temperature dependence of the resistivity for $H\parallel a$ and $I\parallel c$. The two graphs together with Figure 2b illustrate the development of the low-temperature dependence of $\rho(T)$ with $H\parallel a$. The inset in (a) shows the field dependence of $\rho(75 \text{ mK})$ and ρ_0 determined from power-law fits (filled circles).

duction electrons. In a material like YbAgGe, low-energy excitations at low temperatures include particle-hole excitations or magnetic excitations (e.g. spin fluctuations); phonons can be neglected. If $\Delta\rho(T')$ grows, e.g., due to a magnetic-field change, this indicates a softening of some low-energy excitations. Therefore, magnetic critical fluctuations should lead to an increase of $\Delta\rho(T')$ at low T' . A typical quantity to measure the strength of the low-temperature dependence would be the T^2 coefficient A of a quadratic fit $\rho = \rho_0 + AT^2$. For not too strong interactions Fermi liquid theory holds and magnetic excitations can be reexpressed as renormalised particle-hole excitations. However, for YbAgGe $\Delta\rho \propto T^2$ only in a limited high-field range. From $H\parallel a = 14 \text{ T}$ to $H\parallel a = 11 \text{ T}$ the value of A rises by more than a factor 5. For a comparison of the low-temperature dependence of ρ in the whole investigated field range we use the quantity $\Delta\rho(250 \text{ mK})$. Moreover, the field dependence is qualitatively the same for $\Delta\rho(T)$ with, e.g., $T = 150 \text{ mK}$, $T = 250 \text{ mK}$, or $T = 350 \text{ mK}$. $\Delta\rho(250 \text{ mK})$ rises strongly when approach-

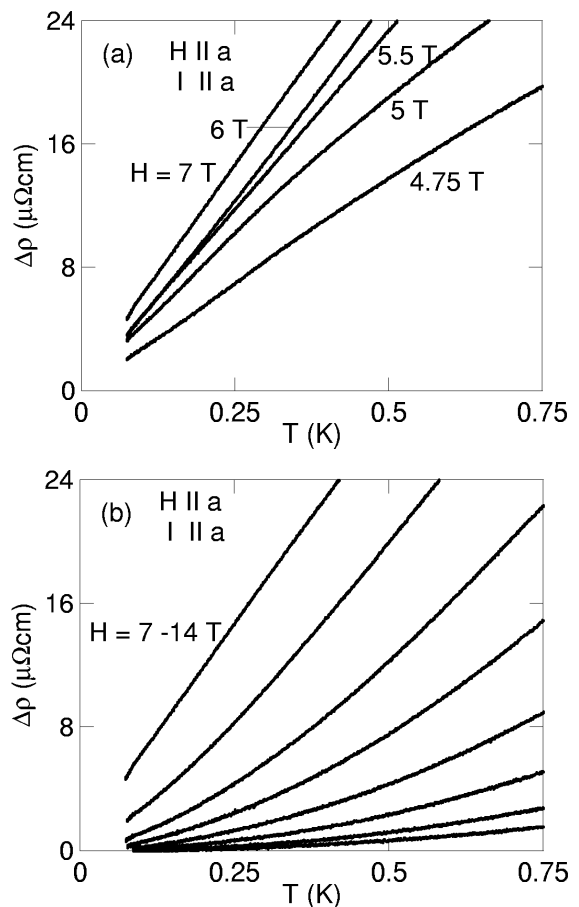


FIG. 5: Temperature dependence of the resistivity for $H\parallel a$ and $I\parallel a$. The two graphs illustrate the development of the low-temperature dependence of $\rho(T)$ with $H\parallel a$.

ing $H\parallel a = 6-7 \text{ T}$. A second peak in $\Delta\rho(250 \text{ mK})$ just below H_{c3}^a , which is very sharp, might be an artefact caused by the feature at $T_3(H)$. Figure 6 shows that the two peaks mark the field range in which n is minimal.

In Figure 7 we visualise the result of the data analysis that $n < 2$ in a considerable range of H^a . $\Delta\rho(T^2)$ at $H\parallel a = 7 \text{ T}$ deviates strongly from a straight line, which would indicate a quadratic temperature dependence (Figure 7a). The more sensitive test of a quadratic temperature dependence $\Delta\rho/T^2(T)$ shows a considerable deviation up to $H\parallel a = 10 \text{ T}$ (Figure 7b). A crossover from conventional Fermi-liquid (FL) to non-Fermi-liquid resistivity (see Figure 12) sets in where $\Delta\rho(T^2)$ curves show deviations from straight lines. The error comes from averaging the crossover temperatures for $I\parallel a$ and $I\parallel c$. Due to the data-noise level, a determination of the resistivity exponent n is only possible above 150 mK. Our results confirm indications for an unconventional resistivity in an extended field range above H_{c3}^a seen in previous resistivity measurements down to 0.4 K.¹⁶

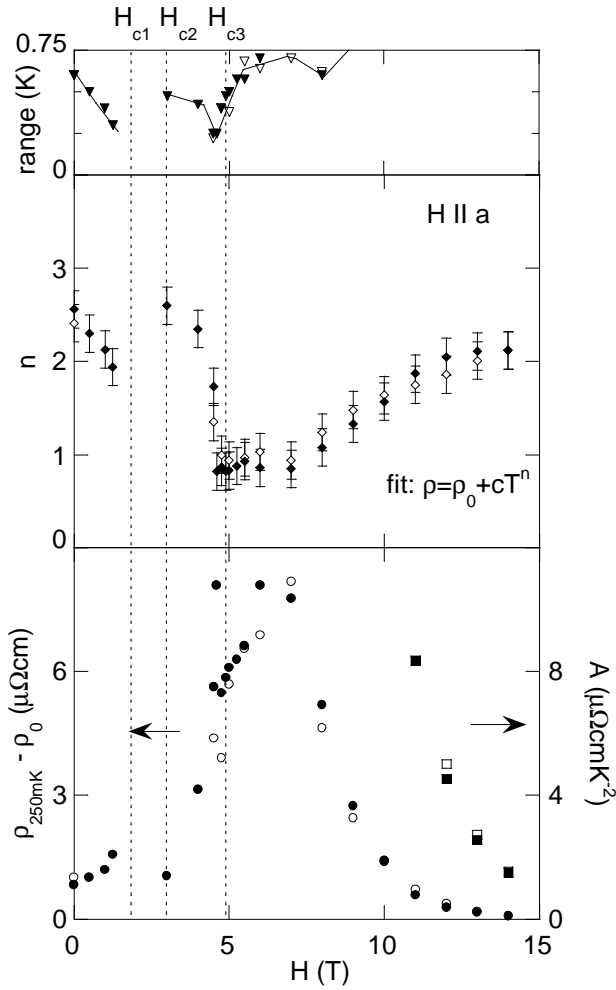


FIG. 6: Analysis of the low-temperature resistivity for $H||a$. Measurements with current $I||a$ (empty symbols) or $I||c$ (filled symbols) give similar results. The low-temperature exponent n (diamonds) results from single-power-law fits of $\rho(T)$. The range, over which the single-power law holds, is indicated in the upper part of the figure (down triangles). Close to H_{c1}^a the jump in the resistivity prevents the determination of n . Below H_{c3}^a n is generally close to or above 2. Between H_{c3}^a and $H||a = 7$ T $n \approx 1$. At higher fields the exponent is increasing to $n \approx 2$. The evolution of the A coefficient (squares) can only be determined at high fields where $n \approx 2$. A is the result of the fit $\rho = \rho_0 + AT^2$ up to 750 mK. In general, the magnitude of the low-temperature dependence is measured by the size of $\Delta\rho(250$ mK) (circles). Note the maxima at $H||a = 4.75$ T and $H||a = 6.5 \pm 0.5$ T. The results of A and $\Delta\rho(250$ mK) for $I||a$ have been scaled down by a factor 0.56. These graphs are the result of analysing data shown in Figures 2, 4, and 5.

B. $H||c$

Now the results for the resistivity of YbAgGe obtained for $H||c$ will be described. We exclusively measured the c -axis resistivity. Figure 8 shows the suppression of the first-order transition with increasing field. At $H||c = 1$ T it still resembles a jump-like drop known from zero-field

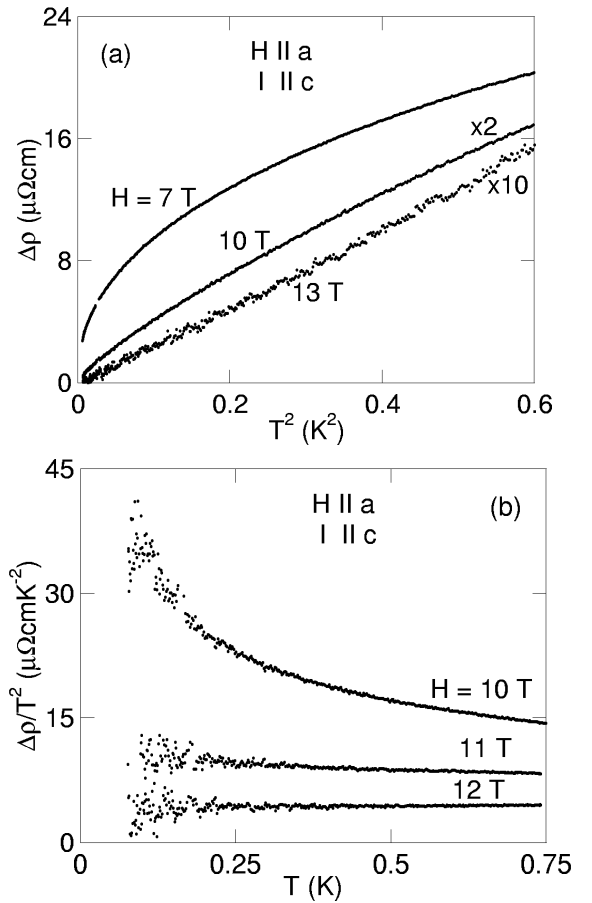


FIG. 7: Deviation of the temperature dependence of the resistivity from quadratic behaviour for $H||a$. (a) At 7 T there is a clear deviation from a T^2 form of $\Delta\rho(T)$. The deviation is reduced towards higher fields. The curves at high fields are shown on reduced scales to allow better comparison of the qualitative temperature dependence. (b) Above 10 T the resistivity becomes quadratic (horizontal line of $\Delta\rho/T^2$ vs T). In this case, $\Delta\rho/T^2$ corresponds to the A coefficient.

measurements and measurements with $H||a$. This jump is suppressed to lower temperatures with increasing $H||c$. However, from 2 T onwards the jump becomes considerably washed out. At the same time a shoulder appears at temperatures clearly below the position of the washed out jump. With increasing $H||c$ this shoulder becomes more clearly visible but suppressed in temperature as well. At $H||c = 5$ T the signature of the first transition can no longer be detected above 70 mK. No clear features of the second-order transition can be detected in $\rho(T)$ at higher fields. In $\rho(H||c)$, however, two transitions are visible: the transition field of the first-order transition $H_1^c(T)$ is marked by the onset of a drop in $\rho(H||c)$ towards lower fields and the transition field $H_3^c(T)$ at higher fields is marked by a shoulder (Figure 9). This transition is denoted as $H_3^c(T)$ and T_3 because of the similar features in $\rho(H)$ and the low-temperature Hall resistivity²¹ that are used to identify it (in analogy to the $H||a$ data). The

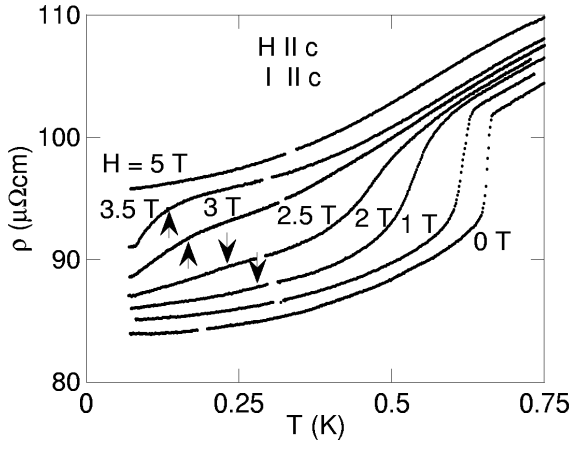


FIG. 8: Signatures of magnetic phase transitions in $\rho(T)$ for $H\parallel c$. The first transition (T_1 , onset of a drop of ρ) is suppressed with field and fully disappears at 5 T. The suppression does not happen continuously. At 2 T and above, the jump-like drop gets washed out and a shoulder (T^* , indicated by arrows) occurs.

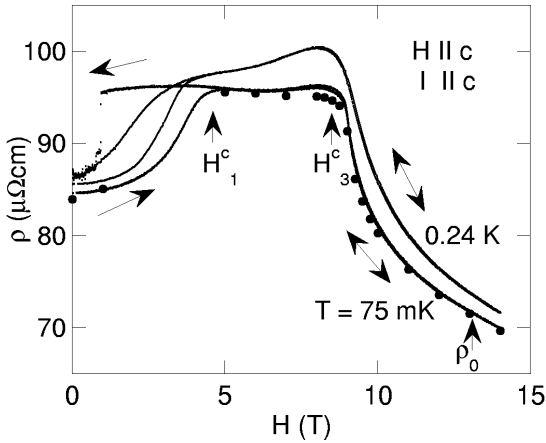


FIG. 9: Signatures of the two magnetic phase transitions in $\rho(H\parallel c)$ at low temperatures. The large arrows indicate the directions of the field sweeps. The sweeps show the clear first order character of the first transition. Due to the small temperature dependence of ρ below 100 mK, the field sweeps at 75 mK are very similar to $\rho_0(H\parallel c)$ determined from power-law fits (filled circles). The difference between $\rho(H)$ at 75 mK and 240 mK illustrates the $H\parallel c$ dependence of the strength of the low-temperature resistivity.

hysteresis in $\rho(T)$ around H_1^c is further evidence for the first-order character of the first transition. The signatures for phase transitions in $\rho(T, H\parallel c)$ are summarised in the H^c - T phase diagram (Figure 12b). The onset of the drop of $\rho(H\parallel c)$ towards lower fields seems to correspond to the jump-like feature (T_1) in $\rho(T)$, marking at low fields the transition from region I to III (which corresponds to the transition between AF1 and AF2 order at zero field). However, from $H\parallel c = 2$ T onwards, at

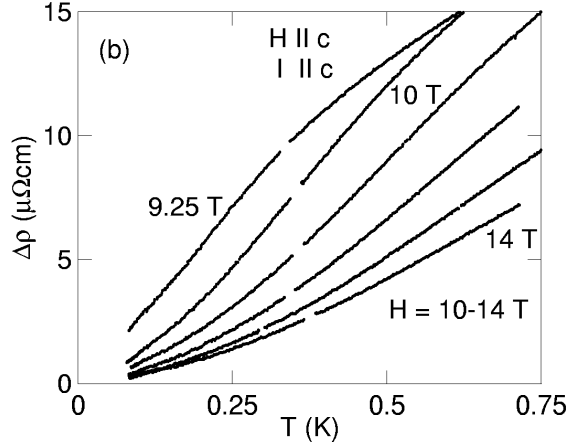
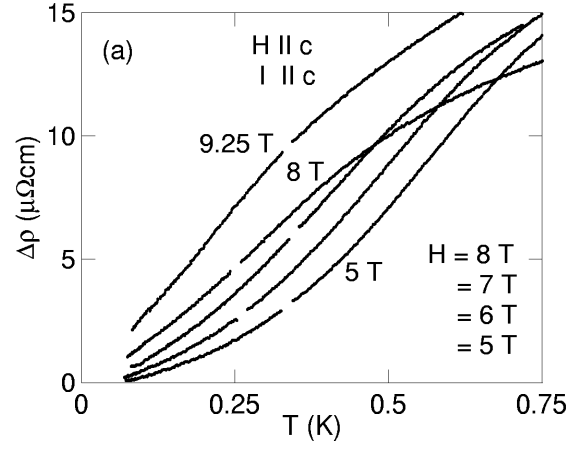


FIG. 10: Temperature dependence of the resistivity for $H\parallel c$. The two graphs illustrate the development with field of the low-temperature dependence of $\rho(T)$, which is strongest at 9.25 T.

T^* separating region I and II, YbAgGe might undergo some transition or crossover (indicated by the shoulder-like feature in $\Delta\rho(T)$). The critical field of region I is $H_{c1}^c = 4.4 \pm 0.1$ T. Above H_{c1}^c , region III extends to $H_{c3}^c = 8.8 \pm 0.1$ T. The results of this study extend previous results from thermodynamic and transport measurements down to 0.4 K (see discussion section) and agree well with previous results in the overlap region.¹⁶

The $H\parallel c$ dependence of $\rho(75$ mK) and ρ_0 (Figure 9) are similar on the shown large resistivity scale. A strong drop of ρ_0 towards high fields is observed.

The $H\parallel c$ dependence of the low-temperature dependence of $\Delta\rho$ can be seen in Figure 10. The magnitude (slope) of the low-temperature dependence of $\Delta\rho$ is generally increasing at lower fields. At $H\parallel c = 9.25$ T it is reaching a maximum and then decreasing towards high fields. To discuss the field dependence of $\Delta\rho$ more quantitatively, ρ has again been fitted with a general power law of the form $\rho = \rho_0 + cT^n$ and $n(H\parallel c)$ is shown in Figure 11. For finite $H\parallel c < 7$ T n is close to the Fermi-liquid value 2. Towards H_{c3}^c the temperature exponent is falling to $n \approx 1.0 \pm 0.2$ in an interval of 1 T around the

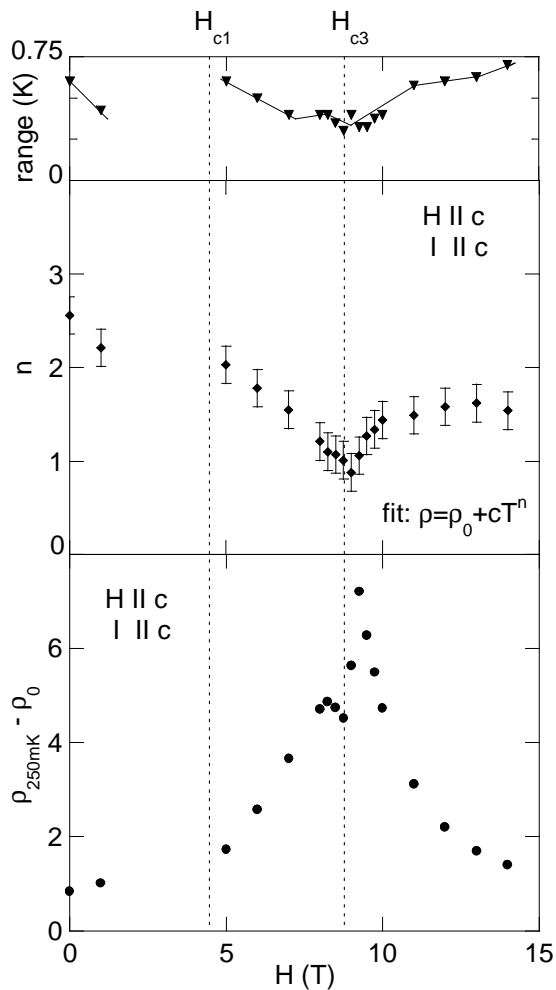


FIG. 11: Analysis of the low-temperature resistivity for $H||c$. The low-temperature exponent n results from single-power-law fits of $\rho(T)$ (diamonds). The range, over which the single-power law holds, is indicated in the upper part of the Figure (down triangles). Close to H_{c1}^c the shoulder in $\rho(T)$ does not allow a determination of n . In the AF1 phase $x \geq 2$. At higher fields $n < 2$ in a considerable range with a minimum $n \approx 1$ close to H_{c3}^c . The magnitude of the low-temperature dependence of $\rho(T)$ is measured by the size of $\Delta\rho(250 \text{ mK})$ and reaches a maximum close to H_{c3}^c . These graphs are the result of analyzing measurements shown in Figure 10.

critical field. At higher fields $n > 1$ up to 14 T.

Figure 11 also shows the enhancement of the magnitude of the low-temperature dependence of $\Delta\rho$ towards H_{c3}^c . The magnitude of the low-temperature dependence of $\Delta\rho$ is again expressed by the quantity $\Delta\rho(250 \text{ mK})$. An enhancement of $\Delta\rho(250 \text{ mK})$ towards H_{c3}^c is observed, which corresponds to the field range where $n \approx 1$. The existence of two peaks around H_{c3}^c instead of one peak at H_{c3}^c might be an artefact caused by the signal of the second transition. Our results confirm indications for Non-Fermi-liquid (NFL) resistivity in an extended field range close to and above H_{c3}^c seen in previous resistivity measurements down to 0.4 K.¹⁶

IV. DISCUSSION

First we interpret briefly the $H - T$ phase diagram obtained for YbAgGe (Figure 12). The transition at T_1 is first order, as is most evident from the large hysteresis in $\rho(H||c)$ (Figure 9). Temperature exponents $n > 2$ found in the spontaneously ordered phases (Figures 6 and 11) indicate scattering from spin waves. Spin waves are present, if the characteristic temperature for the freezing out of spin waves, which is determined by the band splitting in the magnetically ordered phases, is small enough. Considering that at 1 K only a small amount of entropy was detected in heat-capacity measurements at zero field the ordered moment in the AF1 phase and the related band splitting should be small and the presence of spin waves likely. However, no spin-wave excitations have been found so far in inelastic neutron experiments.¹⁹ Around the other lines in the phase diagram no hysteretic behaviour has been found. Neutron scattering measurements suggest a suppression of the AF2 phase at T_2 via a second order transition.²⁰ It has yet to be clarified, whether the features at T^* and T_3 correspond to crossovers or phase transitions. Therefore, the existence of QCPs at the corresponding critical fields is possible.

A main aim of the presented work was to study in detail the development of unconventional material properties in approaching the critical fields in YbAgGe. The results for the field and temperature dependent resistivity $\rho(T, H)$ should serve to address the question whether a magnetic field-induced QCP is present in this material. Indeed, ρ indicates the existence of a field-induced QCP in YbAgGe in two ways when approaching the vicinity of the highest critical field: (i) the temperature dependence of resistivity measured by $\Delta\rho(250 \text{ mK})$ is strongly increased and (ii) the temperature exponent n decreases to 1, i.e. clearly dropping below the Fermi-liquid value. Currently, detailed predictions for the resistivity in the vicinity of a field-induced QCP are still lacking. However, the unconventional features observed in the resistivity of YbAgGe resemble qualitatively predictions for the resistivity of a material which is tuned through a QCP at zero field. In the spin-density wave scenario, the low-temperature exponent n is predicted to be below 2 at the critical point and can be as low as 1 depending on the dimensionality $D + z$ of the spin system, where D is the number of spatial dimensions and z the dynamical exponent.^{22,23,24,25} Antiferromagnetic fluctuations act only as scatterers of quasiparticles from the so-called hot regions of the Fermi surface and $n = 2$ for perfectly pure samples. However in the limit $\Delta\rho(T)/\rho_0 \ll 1$, which is relevant for this measurement, effects from short-circuiting of hot regions are insignificant.^{26,27,28} A linear resistance is predicted for three-dimensional electrons coupled to two-dimensional critical fluctuations.²⁹ Furthermore, in the spin-density-wave scenario a strong increase of the general temperature dependence of the resistivity is expected close to the QCP due to scattering

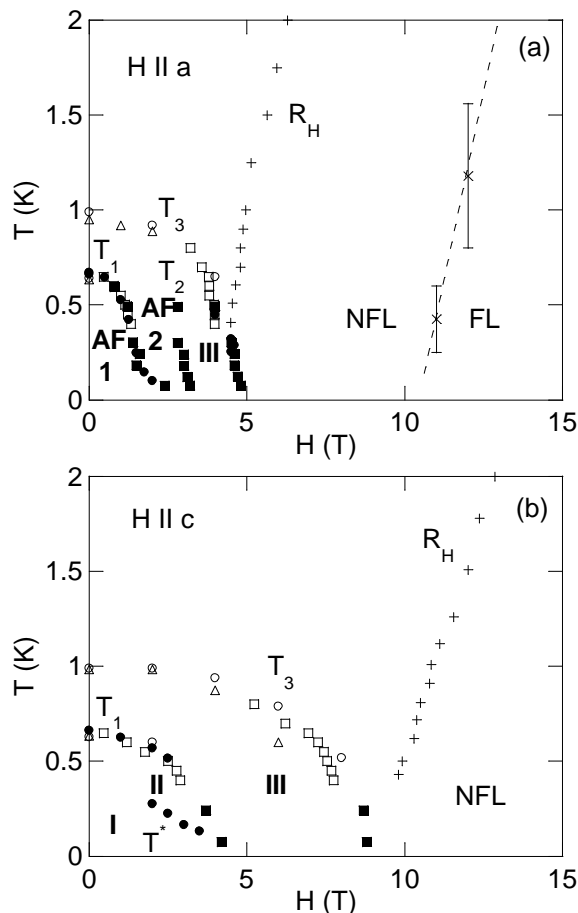


FIG. 12: Field-temperature phase diagrams of YbAgGe. The magnetic phase boundaries are mapped by combining results of this study (representative data sets shown in Figures 2, 3, 8, and 9; filled symbols) and a recent study (empty symbols).¹⁶ Indications for phase transitions have been seen in the resistivity (from up-sweeps in T , circles), the magnetoresistance (from up-sweeps in H , squares), and in the specific heat (triangles). Features in the Hall resistivity (crosses, R_H) define a further line in the phase diagrams.²¹ (a) For $H||a$ at lower fields two antiferromagnetic phases (AF1 and AF2) are found, as well as region III with yet unknown magnetic properties, and a high field regime. The crossover in the high-field regime between non-Fermi-liquid (NFL) and Fermi-liquid (FL) resistivity sets in where $\Delta\rho(T^2)$ ceases to follow a straight line. This phase diagram is the combined result of the in-plane and c -axis resistivity. (b) For $H||c$, the various order parameters are unknown but region I and III correspond to AF1 and AF2 order at zero field, respectively. At high fields an NFL regime is found.

from a strongly increased amount of fluctuations of softened magnetic modes. We add that $\Delta C/T$ of YbAgGe does not saturate in measurements down to 0.4 K.¹⁶ This pattern of unconventional low-temperature resistivity and heat capacity has been observed a number of times in, e.g., heavy fermion systems or weakly magnetic d -metals when approaching a zero-field QCP by changing the chemical composition or applying pressure.

The observation of an NFL resistivity to low temperatures in a wide field region is unusual even in the context of field-induced quantum criticality. There are no indications for phase transitions at the high-field side of H_{c3}^a or H_{c3}^c and therefore the wide NFL range is not created by two nearby QCPs. Local variations of the magnetic properties due to impurities or defects might not be a good explanation of the wide NFL range either, considering the sharpness of the first-order transition. MnSi shows deviations from Fermi-liquid resistivity in a wide pressure range^{30,31,32,33} but the relevant underlying physics close to a first-order transition to a helimagnetic state appears to be quite different from the mechanisms important in YbAgGe close to H_{c3} . However, we note that the NFL range matches the field range, over which ρ_0 drops strongly and beyond which the magnetic susceptibility is strongly reduced.¹⁶ Such behaviour has been observed in other rare-earth metals like CeAl₂ or CePb₃ (Refs. 34,35) and marks the regime of competition between internal magnetic interactions and the Zeeman effect caused by the external magnetic field. Given the large field dependence of ρ_0 in the intermediate field regime, it will be interesting to study the impurity dependence of the NFL range.

In YbAgGe, antiferromagnetic order at low magnetic fields suggests the importance of antiferromagnetic interactions in this material. The competition between internal antiferromagnetic interactions and the Zeeman interaction is likely to be at the origin of enhanced critical fluctuations. Currently, it is unclear by which model the spectrum of the critical fluctuations can be best described. Apart from the spin-density-wave scenario the local character of the f -electrons might be important to categorise a QCP in YbAgGe taking into account the low Kondo temperature $T_K \approx 25$ K.^{14,15} In this respect YbAgGe could turn out to be similar to CeCu_{6-x}Au_x at its zero-field QCP, or similar to YbRh₂Si₂ at its QCP near zero-field. There unconventional transport and thermodynamic properties are assigned to the strong localisation of the f -electrons in these systems.^{13,36} We note the formal similarity in the phase diagram of YbRh₂Si₂ and YbAgGe that a feature in the hall resistivity defines a line which originates from the critical field for the suppression of magnetism.^{21,37} Finally, frustration effects in the quasi-Kagome planes might be a relevant ingredient to the fluctuation spectrum of YbAgGe. The fluctuation spectrum has to be studied directly by in-field neutron scattering measurements and in-field heat capacity measurements below 0.4 K to learn more about the nature of the low-energy excitations in YbAgGe. The impurity-level dependence of the size of the field range, where YbAgGe shows non-Fermi-liquid resistivity, should also be investigated.

V. CONCLUSION

The presented measurements of the field and temperature dependent resistivity of single crystals of hexagonal YbAgGe up to 14 T allow to extend the $H - T$ phase diagrams down to 70 mK. In particular, for the field applied along the crystallographic a-axis, the critical fields for the suppression of two antiferromagnetic phases have been determined to be $H_{c1}^a \approx 2$ T, $H_{c2}^a = 3.0 \pm 0.1$ T. A further phase is suppressed at $H_{c3}^a = 4.9 \pm 0.1$ T. For the field applied along the crystallographic c-axis, critical fields for the suppression of phases, which show AF1 order and AF2 order at zero field, are $H_{c1}^c = 4.4 \pm 0.1$ T and $H_{c3}^c = 8.8 \pm 0.1$ T, respectively. In the low-field magnetically ordered phases the low-temperature dependence of the resistivity is generally characterised by a temperature exponent n close to or above 2. However, close and beyond the highest critical fields for both field directions unconventional exponents $1 \leq n < 1.5$ describe the low-temperature resistivity, before Fermi-liquid behaviour is

approached at high fields. Since unconventional temperature exponents are accompanied by a strong enhancement of the strength of the low-temperature dependence of $\rho(T)$ our results indicate the existence of field-induced quantum critical fluctuations in YbAgGe whose nature has yet to be specified.

Acknowledgments

We thank B. Fåk, Ch. Rüegg, D. McMorro, A. Huxley, M. Zhitomirsky, H. Tsunetsugu, and M. Continentino for valuable discussions on this topic. One of the authors (PGN) thanks P. Haen for a seminar on magnetoresistance measurements. Ames Laboratory is operated for the U.S. Department of Energy by Iowa State University under Contract No. W-7405-ENG-82. This work was supported by the Director for Energy Research, Office of Basic Energy Sciences.

-
- * e-mail: niklowit@drfmc.ceng.cea.fr
- ¹ P. Haen, J. Flouquet, F. Lapierre, P. Lejay, and G. Remenyi, *J.LowTemp.Phys.* **67**, 391 (1987).
 - ² J. Flouquet, P. Haen, S. Raymond, D. Aoki, and G. Knebel, *PhysicaB* **319**, 251 (2002).
 - ³ S. A. Grigera, R. S. Perry, A. J. Schofield, M. Chiao, S. R. Julian, G. G. Lonzarich, S. I. Ikeda, Y. Maeno, A. J. Millis, and A. P. Mackenzie, *Science* **294**, 329 (2001).
 - ⁴ J. S. Kim, D. Hall, K. Heuser, and G. R. Stewart, *Solid-StateComm.* **114**, 413 (2000).
 - ⁵ K. H. Kim, N. Harrison, M. Jaime, G. S. Boebinger, and J. A. Mydosh, *Phys.Rev.Lett.* **91**, 256401 (2003).
 - ⁶ J. S. Kim, N. O. Moreno, J. L. Sarrao, J. D. Thompson, and G. R. Stewart, *Phys.Rev.B* **69**, 24402 (2004).
 - ⁷ J. Paglione, M. A. Tanatar, D. G. Hawthorn, E. Boaknin, R. W. Hill, F. Ronning, M. Sutherland, L. Taillefer, C. Petrovic, and P. C. Canfield, *Phys.Rev.Lett.* **91**, 246405 (2003).
 - ⁸ K. Heuser, E.-W. Scheidt, T. Schreiner, and G. R. Stewart, *Phys.Rev.B* **57**, R4198 (1998).
 - ⁹ E.-W. Scheidt, T. Schreiner, K. Heuser, and G. R. Stewart, *PhysicaB* **259-261**, 388 (1999).
 - ¹⁰ G. R. Stewart, *Rev.Mod.Phys.* **73**, 797 (2001).
 - ¹¹ P. Gegenwart, J. Custers, C. Geibel, K. Neumaier, T. Tayama, K. Tenya, O. Trovarelli, and F. Steglich, *Phys.Rev.Lett.* **89**, 56402 (2002).
 - ¹² K. Ishida, K. Okamoto, Y. Kawasaki, Y. Kitaoka, O. Trovarelli, C. Geibel, and F. Steglich, *Phys.Rev.Lett.* **89**, 107202 (2002).
 - ¹³ J. Custers, P. Gegenwart, H. Wilhelm, K. Neumaier, Y. Tokiwa, O. Trovarelli, C. Geibel, F. Steglich, C. Pepin, and P. Coleman, *Nature* **424**, 524 (2003).
 - ¹⁴ E. Morosan, S. L. Bud'ko, P. C. Canfield, M. S. Torikachvili, and A. H. Lacerda, *J.Magn.Magn.Mat.* **277**, 298 (2004).
 - ¹⁵ K. Katoh, Y. Mano, K. Nakano, G. Terui, Y. Niide, and A. Ochiai, *J.Magn.Magn.Mat.* **268**, 212 (2004).
 - ¹⁶ S. L. Bud'ko, E. Morosan, and P. C. Canfield, *Phys.Rev.B* **69**, 14415 (2004).
 - ¹⁷ T. Matsumura, H. Ishida, T. J. Sato, K. Katoh, Y. Niide, and A. Ochiai, *J.Phys.Soc.Jpn* **73**, 2967 (2004).
 - ¹⁸ K. Umeo, K. Yamane, Y. Muro, K. Katoh, Y. Niide, A. Ochiai, T. Morie, T. Sakakibara, and T. Takabatake, *J.Phys.Soc.Jap.* **73**, 537 (2004).
 - ¹⁹ B. Fåk, D. F. McMorro, P. G. Niklowitz, S. Raymond, E. Ressouche, J. Flouquet, P. C. Canfield, S. L. Bud'ko, Y. Janssen, and M. J. Gutmann, *J.Phys.:Cond.Mat.* **17**, 301 (2005).
 - ²⁰ B. Fåk, C. Rüegg, P. G. Niklowitz, D. F. McMorro, J. Flouquet, P. C. Canfield, S. L. Bud'ko, Y. Janssen, and K. Habicht, submitted to the Conference Proceedings of SCES'05, Vienna, *Physica B*.
 - ²¹ S. L. Bud'ko, E. Morosan, and P. C. Canfield, *Phys.Rev.B* **71**, 054408 (2005).
 - ²² J. A. Hertz, *Phys.Rev.B* **14**, 1165 (1976), and references therein.
 - ²³ A. J. Millis, *Phys.Rev.B* **48**, 7183 (1993), and references therein.
 - ²⁴ T. Moriya, *Spin Fluctuations in Itinerant Electron Magnetism* (Springer, Berlin, 1985), and references therein.
 - ²⁵ G. G. Lonzarich, *Electron* (Cambridge University Press, Cambridge, 1997), chap. 6.
 - ²⁶ R. Hlubina and T. M. Rice, *Phys.Rev.B* **51**, 9253 (1995).
 - ²⁷ A. Rosch, *Phys.Rev.Lett.* **82**, 4280 (1999).
 - ²⁸ A. Rosch, *Phys.Rev.B* **62**, 4945 (2000).
 - ²⁹ A. Rosch, A. Schröder, O. Stockert, and H. v. Löhneysen, *Phys.Rev.Lett.* **79**, 159 (1997).
 - ³⁰ C. Thessieu, C. Pfleiderer, A. N. Stepanov, and J. Flouquet, *J.Phys.Cond.Mat.* **9**, 6677 (1997).
 - ³¹ C. Pfleiderer, G. J. McMullan, S. R. Julian, and G. G. Lonzarich, *Phys.Rev.B* **55**, 8330 (1997).
 - ³² C. Pfleiderer, S. R. Julian, and G. G. Lonzarich, *Nature* **414**, 427 (2001).
 - ³³ N. Doiron-Leyraud, I. R. Walker, L. Taillefer, M. J.

- Steiner, S. R. Julian, and G. G. Lonzarich, *Nature* **425**, 595 (2003).
- ³⁴ F. Lapierre, P. Haen, A. Briggs, and M. Sera, *J.Magn.Magn.Mat.* **63-64**, 76 (1987).
- ³⁵ U. Welp, P. Haen, G. Bruls, G. Remenyi, J. Flouquet, P. Morin, A. Briggs, G. Cors, and M. Karkut, *J. Magn.Magn.Mat.* **63-64**, 28 (1987).
- ³⁶ A. Schröder, G. Aeppli, R. Coldea, M. Adams, O. Stockert, H. Löhneysen, E. Bucher, R. Ramazashvili, and P. Coleman, *Nature* **407**, 351 (2000).
- ³⁷ S. Paschen, T. Lühmann, S. Wirth, P. Gegenwart, O. Trovarelli, C. Geibel, F. Steglich, P. Coleman, and Q. Si, *Nature* **432**, 881 (2004).